HHS Public Access

Author manuscript

J Vasc Interv Radiol. Author manuscript; available in PMC 2024 July 01.

Published in final edited form as:

J Vasc Interv Radiol. 2023 July ; 34(7): 1247–1257.e8. doi:10.1016/j.jvir.2023.03.016.

Treatment of Hepatocellular Carcinoma by Multimodal In Situ Vaccination Using Cryoablation and a Plant Virus Immunostimulant

Mansur A. Ghani, MD,
Department of Radiology, University of California San Diego, La Jolla, California

Amandip Bangar, BS,
Department of Radiology, University of California San Diego, La Jolla, California

Yunpeng Yang, MD,
Department of Radiology, University of California San Diego, La Jolla, California

Eunkyeong Jung, PhD,
Department of NanoEngineering, University of California San Diego, La Jolla, California

Consuelo Sauceda, BS,
Department of Pharmacology, Skaggs School of Pharmacy and Pharmaceutical Sciences, University of California San Diego, La Jolla, California

Tyler Mandt, MD,
Department of Radiology, University of California San Diego, La Jolla, California

Sourabh Shukla, PhD,
Department of NanoEngineering, University of California San Diego, La Jolla, California

Nicholas J.G. Webster, PhD,
Division of Endocrinology and Metabolism, Department of Medicine, Moores Cancer Center, VA San Diego Healthcare System, University of California San Diego, La Jolla, California

Nicole F. Steinmetz, PhD,
Department of Radiology, Department of NanoEngineering, Moores Cancer Center, Department of Bioengineering, Center for Nano-ImmunoEngineering, Institute for Materials Discovery and Design, University of California San Diego, La Jolla, California

Isabel G. Newton, MD, PhD
Department of Radiology, VA San Diego Healthcare System, University of California San Diego, La Jolla, California

Abstract

Address correspondence to I.G.N., Department of Radiology, University of California San Diego, 200 W Arbor Dr. MC 8756, San Diego, CA 92103-1911; inewton@health.ucsd.edu; Twitter handle: @theIIMD.

From the 2023 SIR Annual Scientific Meeting (Abstract No. 6, “Treatment of HCC by Multimodal In Situ Vaccination Using Cryoablation and a Plant Virus Immunostimulant”).

Figures E1–E6, Tables E1–E3, and Appendix A can be found by accessing the online version of this article on www.jvir.org and selecting the Supplemental Material tab.

Purpose: To test the hypothesis that cryoablation combined with intratumoral immunomodulating nanoparticles from cowpea mosaic virus (CPMV) as an in situ vaccination approach induces systemic antitumoral immunity in a murine model of hepatocellular carcinoma (HCC).

Materials and Methods: Mice with bilateral, subcutaneous RIL-175 cell–derived HCCs were randomized to 4 groups: (*a*) phosphate-buffered saline (control), (*b*) cryoablation only (Cryo), (*c*) CPMV-treated only (CPMV), and (*d*) cryoablation plus CPMV-treated (Cryo + CPMV) (N = 11–14 per group). Intratumoral CPMV was administered every 3 days for 4 doses, with cryoablation performed on the third day. Contralateral tumors were monitored. Tumor growth and systemic chemokine/cytokine levels were measured. A subset of tumors and spleens were harvested for immunohistochemistry (IHC) and flow cytometry. One- or 2-way analysis of variance was performed for statistical comparisons. A *P* value of <.05 was used as the threshold for statistical significance.

Results: At 2 weeks after treatment, the Cryo and CPMV groups, alone or combined, outperformed the control group in the treated tumor; however, the Cryo + CPMV group showed the strongest reduction and lowest variance (1.6-fold ± 0.9 vs 6.3-fold ± 0.5, $P < .0001$). For the untreated tumor, only Cryo + CPMV significantly reduced tumor growth compared with control (9.2-fold ± 0.9 vs 17.8-fold ± 2.1, $P = .01$). The Cryo + CPMV group exhibited a transient increase in interleukin-10 and persistently decreased CXCL1. Flow cytometry revealed natural killer cell enrichment in the untreated tumor and increased PD-1 expression in the spleen. Tumor-infiltrating lymphocytes increased in Cryo + CPMV–treated tumors by IHC.

Conclusions: Cryoablation and intratumoral CPMV, alone or combined, demonstrated potent efficacy against treated HCC tumors; however, only cryoablation combined with CPMV slowed the growth of untreated tumors, consistent with an abscopal effect.

Hepatocellular carcinoma (HCC) is the fourth leading cause of cancer-related death worldwide, and its incidence in the United States has almost tripled in 30 years (1). HCC evades immune detection through various mechanisms, which immunotherapy aims to reverse (2). Because of the immunosuppressive tumor microenvironment (TME) in HCC, combining immunotherapy with liver-directed therapies may constitute a robust in situ vaccination (ISV) approach.

Cryoablation may be a viable component of multimodal ISV therapies because it releases undenatured tumor-associated antigens (TAAs) for uptake and presentation by dendritic cells and increases the levels of proinflammatory cytokines and transcription factors, such as interleukin (IL)-1, nuclear factor kappa B, and tumor necrosis factor α (3,4). Rarely, cryoablation induces a systemic, antitumoral response culminating in the disappearance of metastatic disease (ie, “abscopal effect”), as observed in melanoma, lung cancer, and breast cancer (5–7). For HCC, combining cryoablation with immunoadjuvants to overcome the immunosuppressive TME may facilitate an abscopal effect.

Immunoadjuvants promote immune recognition and uptake of TAAs by dendritic cells. This process may link the innate and adaptive antitumoral immune responses, which is necessary for the abscopal effect (8). The immunoadjuvant cowpea mosaic virus (CPMV)-derived nanoparticles are derived from the 30-nm, nonenveloped plant virus that carries a bipartite

single-stranded RNA genome. CPMV cannot infect mammals. Intratumoral CPMV induces systemic, durable antitumoral immunity in mouse models of melanoma, ovarian cancer, breast cancer, and glioma (9–14) as well as companion dogs with melanoma, sarcoma, and mammary tumors (15,16). CPMV promotes an immunogenic TME by activating multiple toll-like receptors and recruiting and activating innate immune cells (eg, neutrophils and macrophages) and natural killer (NK) cells that process TAAs, leading to lasting, adaptive antitumoral immunity and immune memory (12,17). This study combines intratumoral CPMV with cryoablation to test the hypothesis that this novel, multimodal ISV approach stimulates systemic antitumoral immunity against HCC.

MATERIALS AND METHODS

CPMV Particle Preparation

CPMV was propagated in California Blackeyed No. 5 cowpea plants (Morgan County Seeds, Barnett, Missouri) and was harvested, purified, and characterized, as previously described (18). In brief, the primary leaves were dusted with carborundum and mechanically inoculated with 0.05-mg virus/leaf. The infected primary leaves and trifoliates were then harvested (10–15 days after inoculation), and CPMV was purified by chloroform-butanol extraction, polyethylene glycol precipitation, and sucrose gradient ultracentrifugation. CPMV was characterized by sodium dodecyl sulfate–polyacrylamide gel electrophoresis, size exclusion chromatography using a Superose 6 Increase column and fast liquid protein chromatography (CytoViva, Auburn, Alabama), and transmission electron microscopy.

Cell Culture

RIL-175 cells (from Dr. Timothy Greten, National Cancer Institute) were previously isolated from hepatic tumors established in C57BL/6 mice via transfer of $p53^{-/-}$ fetal hepatoblasts transduced with $HRas^{V12}$ (19). Cells were maintained in Dulbecco's Modified Eagle's Medium (10-013-CV-1; Corning, Corning, New York) supplemented with 1% penicillin-streptomycin solution (30-002-CI-1; Corning), 1% Minimal Essential Media Non-Essential Amino Acids Solution (11140050; Thermo Fisher Scientific, Waltham, Massachusetts), and 10% heat-inactivated fetal bovine serum (16140071; Thermo Fisher Scientific) in a humidified 5% CO_2 incubator and passaged at 1:3 every 2–3 days.

Study Design and HCC Tumor Model

All animal experiments were approved by the UC San Diego Institutional Animal Care and Use Committee. This study included 60 male wild-type C57BL/6 mice (The Jackson Laboratory, Bar Habor, Maine) on the basis of a power analysis using G*Power 3.1 (Heinrich Heine University, Düsseldorf, Germany), with an effect size of 0.80 estimated from pilot data, an error probability of 0.05, and a power of 0.85, yielding a calculated total sample size of 8 per group plus 4 mice to account for engraftment failure plus 4 mice for histological/flow cytometric analysis, for a sample size of 15 per group. To induce hepatic steatosis, the mice were fed a nonalcoholic steatohepatitis–inducing Western Diet (D12079; Research Diets, New Brunswick, New Jersey) beginning at 8–10 weeks old for at least 4 weeks. Hepatic steatosis helps establish the systemic, metabolic, and immunologic environment in which HCC arises and may improve rates of RIL-175 tumor engraftment.

Only male mice were included because females demonstrated poorer engraftment possibly due to greater immune recognition to the RIL-175 cell, which originated in a male mouse. The subcutaneous RIL-175 tumor model was chosen to study metastatic HCC because of its baseline immunologic profiles, including key immunosuppressive pathways, which are broadly representative of human HCC (20). Isoflurane anesthesia was administered by nose cone, and the flanks were shaved and then sanitized with iodine solution. For the primary tumor slated for treatment, the right flank was injected subcutaneously (22-gauge needle) with 2.5×10^5 RIL-175 cells suspended in 25 μL of Cultrex Basement Membrane Extract (Sigma-Aldrich, Burlington, Massachusetts). For the untreated tumor, the left flank was injected subcutaneously with a 1.25×10^5 RIL-175 cell suspension so that tumor growth would not limit experiment duration.

Ultrasound-Guided Percutaneous Cryoablation and Intratumoral CPMV Injection

Ten days after tumor inoculation, mice were randomized into 1 of 4 groups: (*a*) phosphate-buffered saline (PBS)-injected (control), (*b*) CPMV-treated (CPMV), (*c*) cryoablation-treated (Cryo), and (*d*) cryoablation plus CPMV-treated (Cryo + CPMV). Tumors were measured with digital calipers at this time and every 3 days thereafter, and the length (greatest diameter) and width (diameter orthogonal to length) were recorded. The volume was calculated by the modified ellipsoidal formula: $V = 1/2 \times (\text{length} \times \text{width}^2)$. Mice with tumors <85 mm^3 in volume at the time of treatment were excluded from analysis. One mouse in the CPMV group that unexpectedly died immediately after the procedure was also excluded, resulting in a total of 11–14 mice per group. Mice with a primary tumor that did meet the size criteria but a secondary tumor that did not meet the size criteria were still treated; however, only the primary tumor was included for analysis. On Days 0, 3, 6, and 9, the primary tumor was injected (26-gauge needle) with 20-μL CPMV (5 μg/μL) (CPMV and Cryo + CPMV groups) or PBS (control and Cryo groups). On Day 3, the primary tumors in the Cryo and Cryo + CPMV groups were treated with cryoablation using a custom 3-cm, 17-gauge Iceseed cryoprobe (Galil Medical Cryoablation System; Boston Scientific, Marlborough, Massachusetts) placed percutaneously under ultrasound (US) guidance with a 71-MHz US transducer (Vevo MD Ultra High Frequency US system; VisualSonics, Fujifilm, Ontario, Canada) and subjected to 2 cycles of 1-minute active freezes and 1-minute active thaws at 25% power to generate a 7-mm ablation zone. Figure 1 summarizes the study design, sample size allocation, and treatment schedule.

Mice were weighed at the time of tumor cell injection and every 3 days until euthanasia. Moribund animals were euthanized prior to established end points if the tumor volume reached 1 cm^3 or the body weight decreased below baseline by 15%. The Animal Research: Reporting of In Vivo Experiments (ARRIVE) Guidelines Supplement in Appendix A (available online on the article's Supplemental Material page at www.jvir.org) contains additional study design details, including experimental group allocation and exclusion.

Chemokine/Cytokine Analysis

Tail bleed samples were collected in ethylenediaminetetra-acetic acid tubes at Days 0, 3, and 6, and samples were centrifuged at 6,000 rpm for 6 minutes at 4 °C. The supernatant was stored at −80 °C prior to analysis using an electrochemiluminescence-based multiplex

immunoassay on a MESO Quickplex SQ 120MM instrument (Meso Scale Diagnostics, Rockville, Maryland). Interferon-γ, IL-1β, IL-2, IL-4, IL-5, IL-10, IL-12p70, IL-13, CXCL1, and tumor necrosis factor α were measured with the U-plex TH1/TH2 Combo kit (product K15071K, Meso Scale Diagnostics) according to the manufacturer's instructions.

Flow Cytometry

At 7 days after treatment initiation, 2 mice per group were euthanized for flow cytometry by isoflurane anesthesia and cervical dislocation. The spleen and tumors were prepared for flow cytometry, as detailed in Appendix A (available online on the article's Supplemental Material page at www.jvir.org). Data were analyzed using Flowjo (FlowJo, Ashland, Oregon).

Histology

At 7 days after treatment initiation, tumors from 1–2 mice per group were harvested by blunt dissection. Tumors were sectioned and fixed in 4% formaldehyde in PBS and then submitted to the UC San Diego Moores Cancer Center Biorepository and Tissue Technology shared resource for paraffin embedding, thin sectioning, hematoxylin and eosin staining, and immunohistochemistry (IHC) using primary antibodies targeted against murine CD4 (Cat# ab183685; Abcam) and CD8 (Cat# 14-0195-82; Thermo Fisher Scientific). Slides were scanned on a Nanozoomer digital slide scanner (Hamamatsu Photonics, Hamamatsu, Japan) at the UC San Diego School of Medicine Microscopy Core. Positive cell counts were quantitated using the Fiji image processing package (21) at 10× (for overall) and 20× (for central and peripheral) magnification and divided by the total quantitated area to determine the positive cell count per square millimeter.

Data Analysis and Statistical Methods

One- or 2-way analysis of variance was performed in Prism (GraphPad, San Diego, California) for all statistical comparisons among treatment groups, with Tukey post hoc tests for multiple comparisons. Flow cytometry data were imported into Prism for statistical analysis. A P value of <.05 was used as the threshold for statistical significance.

RESULTS

Cryo + CPMV Inhibited Growth of Both the Treated and Untreated Tumors

Tumor growth curves for treated and untreated tumors are shown in Figure E1a, b (available online at www.jvir.org). Additional descriptive statistics given in Table E2 (available online at www.jvir.org). All 3 treatment groups demonstrated slower tumor growth than that observed in the control group, with the most profound growth retardation in the Cryo + CPMV group at 2 weeks after the treatment: Cryo + CPMV vs control, 1.6 ± 0.9 vs 6.3 ± 0.5; P < .0001 (Fig 2). A trend toward more profound tumor growth inhibition with Cryo + CPMV than with Cryo or CPMV alone did not reach statistical significance. Analysis of the variance in treatment response revealed lower variance and more consistent response after Cryo + CPMV than after each treatment alone (F-test of Cryo + CPMV vs CPMV, 0.82 vs 6.52; P = .006, and Cryo + CPMV vs Cryo, 0.82 vs 5.65; P = .01) (Fig E2, available online at www.jvir.org).

For the untreated tumor, only the Cryo + CPMV group demonstrated significant growth reduction compared with control (9.2 ± 0.9 vs 17.8 ± 2.1, $P = .01$) (Fig 3); the other groups showed trends toward decreased growth. Additional descriptive statistics are given in Table E3 (available online at www.jvir.org).

Cytokine/Chemokine Analysis Showed Transient Immunosuppression and Then Immunostimulation after Cryo + CPMV

Plasma was assayed for a panel of chemokines and cytokines (Table E1, available online at www.jvir.org). IL-10 and CXCL1, both immunosuppressive, demonstrated statistically significant changes. At Day 3 after Cryo + CPMV, the IL-10 level transiently increased compared with that in the Cryo group (20.0 pg/mL ± 2.7 vs 9.6 pg/mL ± 1.0, $P = .03$) (Fig E3a, available online at www.jvir.org). The trend toward the increased IL-10 level in CPMV-treated mice did not reach statistical significance. At Day 6 after Cryo + CPMV, the CXCL1 level was significantly lower than that in CPMV tumors (98.2 pg/mL ± 17.6 vs 189.0 pg/mL ± 16.6, $P = .01$) (Fig E3b, available online at www.jvir.org). The CXCL1 levels were similar in the control and Cryo groups compared with that in the CPMV group; however, they did not significantly differ from that in the Cryo + CPMV group.

Cryo + CPMV Enriched Immune Cells in Untreated Tumors but Promoted T Cell Exhaustion

Immune cell infiltration into the treated and untreated tumors and spleen was assessed via flow cytometry. Cryo + CPMV increased the $CD4^+$ T cell levels in the untreated tumor compared with Cryo (12.9% vs 8.6%, $P = .03$); both CPMV (8.6% vs 3.6%, $P = .005$) and Cryo + CPMV (7.8% vs 3.6%, $P = .03$) increased the $CD8^+$ T cell levels compared with control (Fig 4). The proportion of $CD8^+/CD137^+$ T cells (ie, $CD8^+$ T cells activated in the presence of antigens) was lower in the treated tumors of CPMV mice (10.9% vs 24.0%, $P = .01$) and Cryo mice (12.0% vs 24.0%, $P = .01$) than in controls. Adding CPMV to Cryo reversed this inhibition (Fig 5a). The $CD8^+/CD137^+$ T cell levels were also lower in the untreated tumors of CPMV mice (18.8% vs 25.4%, $P = .04$) but not in the Cryo + CPMV group (24.6% vs 25.4%, $P = .98$) versus control. PD-1 expression on CD4+ and CD8+ T cells was higher in the spleens of Cryo + CPMV–treated mice than in controls (CD4+, 30.9% vs 10.6%; $P = .007$, and CD8+, 13.7% vs 3.6%; $P = .008$) and Cryo-treated mice (CD4+, 30.9% vs 11.2%; $P = .03$, and CD8+, 13.7% vs 4.0%; $P = .04$) (Fig 5b). NK cells were enriched in the untreated tumors of the Cryo + CPMV group compared with the control group (15.4% vs 8.6%, $P = .04$) and the CPMV group compared with the control (18.3% vs 8.6%, $P = .002$) and Cryo (18.3% vs 10.5%, $P = .009$) groups. NK cells were also enriched in the spleens of the Cryo + CPMV group compared with both the control (6.3% vs 3.7%, $P = .01$) and CPMV (6.3% vs 2.4%, $P = .003$) groups (Fig 5c).

The complete flow cytometry data are shown in Figure E4a–f (available online at www.jvir.org). Statistically significant differences in immune cell populations were generally not found in treated tumors possibly because of lower cells counts after treatment.

Cryo + CPMV Induced a Marked Increase in the Levels of Centrally Penetrating Tumor-Infiltrating Lymphocytes

The overall, peripheral, and central tumor $CD4^+$ and $CD8^+$ lymphocytes were quantified. The overall $CD4^+$ cell levels were highest in the Cryo + CPMV–treated tumors (479/mm^2, $P < .0001$); the overall $CD8^+$ cell levels were higher in the treated tumors of the CPMV (114/mm^2) and Cryo + CPMV (109/mm^2) groups than in the control (39/mm^2) and Cryo (36/mm^2) groups. The center of tumors treated with Cryo + CPMV had dramatically increased the levels of $CD4^+$ cells (664/mm^2) and $CD8^+$ cells (131/mm^2) compared with those in all other groups ($P < .0001$) (Fig 6).

In the untreated tumor, the overall $CD4^+$ cell levels were lowest in the Cryo group (77/mm^2) compared with those in all other groups (control, 177/mm^2; CPMV, 169/mm^2; Cryo + CPMV, 142/mm^2); the overall $CD8^+$ cell levels trended to be higher in the Cryo + CPMV group than in all other groups, without reaching statistical significance (Fig E5a, available online at www.jvir.org). The central $CD4^+$ cell levels were lowest in the Cryo group (8/mm^2) and decreased in the Cryo + CPMV (19/mm^2) versus control (36/mm^2) groups. A trend for increased central $CD8^+$ cell levels in the Cryo + CPMV group compared with those in all other groups did not reach statistical significance (Fig E5b, available online at www.jvir.org). Peripheral cell counts in the treated and untreated tumors (Fig E5c, d, available online at www.jvir.org) were generally in line with the overall results. Figure 7a–d shows the representative examples of $CD4^+$ staining. Tumor fat content was markedly increased only in Cryo + CPMV–treated tumors (Fig 7d).

No Significant Differences in Treatment Toxicity and Weight Loss Were Found between Groups

CPMV-treated animals tended to have lower weight than those in other groups, but these differences did not reach statistical significance (Fig E6, available online at www.jvir.org). No animals reached the 15% weight loss or 1 cm^3 tumor volume threshold for euthanasia or appeared moribund during the 2-week experimental period.

DISCUSSION

Multimodal ISV therapy consisting of cryoablation combined with the immunostimulant CPMV inhibited the growth of both the treated and contralateral, untreated HCC tumors. Although the immune profile changes were mixed, overall, they supported a proimmunogenic TME after combined treatment. Multiparametric flow cytometry and IHC revealed that combination therapy promoted an enrichment of both native and adaptive immune cells, especially in the center of treated tumors, which is characteristic of a shift from an immunologically “cold” to a “hot” tumor.

The potential for clinical translation of this multimodal ISV therapy for patients with intermediate or advanced HCC is promising; however, patients with earlier-stage HCC could also benefit from a reduction in recurrence after ablation through immune elimination of residual cancer cells. This could reduce mortality because sublethal thermal stress stimulates residual cancer cells to proliferate and grow, which can drive more aggressive recurrence

(22). It also supports clinical applications that the multimodal ISV therapy yielded more consistent and reliable tumor growth retardation than cryoablation or CPMV alone.

The immunologic impact of cryoablation may depend on factors such as tumor type, volume of the tumor frozen, and freeze-thaw protocol and whether appropriate immunoadjuvants or costimulatory signaling markers are presented alongside TAAs. Although cryoablation alone may be expected to promote immunostimulation through the release of TAAs and proinflammatory cytokines, this study and studies by others have demonstrated immunosuppressive effects (23). Cryoablation alone decreased the activated $CD8^+$ T cell levels in treated tumors compared with controls by flow cytometry, and there was a relative paucity of intratumoral $CD4^+$ T cells by IHC (ie, cryoablation alone may exacerbate the "cold" immunophenotype). CPMV alone also had a decreased proportion of activated $CD8^+$ T cells in both treated and untreated tumors. These effects were reversed by adding CPMV to cryoablation, supporting that both TAAs and the appropriate signal to induce its uptake and presentation are required for an antitumoral immune response. To explore this further, PD-1 expression was analyzed because RIL-175 hepatoma cells are known to express PD-L1 (24). PD-1 expression on both $CD4^+$ and $CD8^+$ T cells significantly increased in the spleen, which suggests that systemic immune exhaustion occurs with Cryo + CPMV. Thus, a PD-1 inhibitor may enhance the efficacy of this combined treatment. Indeed, a previous study (25) with CPMV in multiple other tumor models found a strong upregulation of checkpoint inhibitors and improved outcomes with the addition of PD-1 inhibitors.

On histology, Cryo + CPMV induced a marked increase in the levels of centrally penetrating tumor-infiltrating lymphocytes (TILs), which characterizes immunogenic (or "hot") tumors. Impaired trafficking of TILs is an immunoevasive strategy by HCC (26). The presence of TILs is strongly associated with an immune-mediated antitumoral response as well as the abscopal effect (27,28). Previous studies (14,25) on CPMV in other tumor models also found marked increases in the levels of $CD4^+$, $CD8^+$, and NK cells in treated tumors; however, the results of this study demonstrated very little tumor-infiltrating ability of immune cells (ie, CPMV alone promotes a "warm" but not "hot" tumor environment). The treatment effect of Cryo + CPMV may, therefore, be related to enhanced TIL recruitment and/or improved tumor permeability to TILs. However, the lack of staining, such as FOXP3, to distinguish between helper T cells and suppressor T cells limits the conclusions about the $CD4^+$ cells. Only Cryo + CPMV–treated tumors demonstrated increased fat, which is often observed after clearance of a tumor. Discrepancies between the histology and flow cytometry data likely reflect technical differences. For example, differences in $CD4^+$ and $CD8^+$ T cell populations in treated tumors by IHC were not observed by flow cytometry. However, the flow cytometry data are expressed in percentage relative to CD45 cells, whereas histology cell counts represent an absolute number.

The IL-10 and CXCL1 levels differed among treatment groups. IL-10 is generally considered an anti-inflammatory cytokine, and its level increased in the Cryo + CPMV group after 3 days, which may reflect a temporary response to curb the inflammation in the TME. CXCL1 is a chemokine that attracts neutrophils and other immune cells during inflammation and promotes angiogenesis and tumor growth in liver cancer (29). CXCL1 also enhances immunotolerance by recruiting immunosuppressive myeloid-derived stem

cells (30). The fact that the CXCL1 level significantly decreased at 6 days in the Cryo + CPMV group compared with those in all other groups suggests a potential antitumoral effect by limiting angiogenesis and relieving immunosuppression. Future studies assessing intratumoral levels of chemokines/cytokines could clarify the significance of these results.

This study has limitations. This subcutaneous tumor model of HCC does not fully recapitulate the microenvironment, treatment effects, and immune status of an intrahepatic tumor. Additionally, the fewer tumor cells inoculated for the smaller untreated tumor resulted in a lower tumor engraftment rate and, therefore, a smaller untreated tumor sample size. The rapid growth of the RIL-175 cells also limited the experimental time period, which could have impacted the magnitude of observable treatment effects. No statistically significant differences were found between the tumor sizes of the Cryo + CPMV group and the Cryo alone or CPMV alone groups. It cannot be excluded that the trend toward smaller treated and untreated tumors in the Cryo + CPMV group reflects subthreshold differences that this study was not powered to detect. In addition, this study was not designed to evaluate for differences in percent tumor necrosis or assess for residual tumor cell quantification between the groups.

In conclusion, combining cryoablation with intratumoral CPMV produced the greatest growth reduction in the treated tumor and demonstrated a modest abscopal effect in the untreated tumor in this model of aggressive HCC. This growth reduction is associated with an enrichment of NK cells in the treated tumor and spleen, increased tumor core–infiltrating $CD4^+$ and $CD8^+$ T cells, and lower CXCL1 levels. The increased expression of PD-1 on $CD4^+$ and $CD8^+$ T cells suggests a role for adding a PD-1 inhibitor in future studies to enhance the efficacy of cryoablation plus CPMV.

Supplementary Material

Refer to Web version on PubMed Central for supplementary material.

ACKNOWLEDGMENTS

The study was supported in part by a Pilot Grant from the Society of Interventional Radiology (to M.A.G.), by grant W81XWH2010742 from Congressionally Directed Medical Research Programs (to N.F.S. and I.G.N.), by grant T32 EB005970 from the National Institutes of Health (to M.A.G.), by grants R01 CA224605 (to N.F.S.) and U01 CA218292 (to N.F.S.), by grants IBX004848 and IBK005224 from the Department of Veterans Affairs (to N.J.G.W.), by a Pilot and Feasibility award from the Moores Cancer Center (to I.G.N. and N.J.G.W.), and a Basic Science Research Program through the National Research Foundation of Korea (NRF) funded by the Ministry of Education, 2022R1A6A3A03066056 (to E.J.).

T.M. reports 2018 Biocompatible UK Research Grant from the Society of Interventional Oncology, 2018 Translational Cancer Research Award from the University of California San Diego Moore's Cancer Center, 2018 to present T32 EB 5970–11 A1 grant from the National Institutes of Health, and 2019 Resident Research Grant from the Radiological Society of North America; reports payment for hotel and travel to the 2022 VIVA/VEINS Conference; and received cryoablation device and custom probes from Boston Scientific/Galil. N.F.S. is a cofounder of, has equity in, and has a financial interest with Mosaic ImmunoEngineering Inc.; serves as Director, Board Member, Acting Chief Scientific Officer, and paid consultant to Mosaic ImmunoEngineering Inc.; reports grant (W81XWH2010742) from the University of California San Diego; report support from Shaughnessy Family Fund (Philanthropy) (to University of California San Diego); and reports the following planned, issued, or pending patents: US App. No. 16/851,778, European App. No. 21201960.8, Chinese App. No. 201580063662.6, Canadian App. No. CA 2967336, Japanese Patent No. 6731405, and Australian Patent No. 2015342790. I.G.N. serves on the Executive Advisory Board for the Interventional Oncology branch of Boston Scientific, which owns Galil, the manufacturer of the cryoablation device used in these experiments; is on the Program Planning

Committee for the Society for Interventional Oncology (SIO); is the Program Director for Western Angiographic and Interventional Society (WAIS); is the Chair of the Board of Directors for the Interventional Initiative; reports travel support from VIVA/VEINS, CARVE, and California Orthopedic Association (COA); reports hotel support from WAIS, SIO, CARVE and COA; is a speaker for Society for Interventional Radiology, VIVA/VEINS, CARVE, and UCSD Graduate Course; is a consultant for AstraZeneca, Genentech, and Replimune; and reports grants from the Department of Defense, UCSD Academy of Clinician Scholars and Society for Interventional Oncology. The other authors have not identified a conflict of interest.

APPENDIX A

ANIMAL RESEARCH: REPORTING OF IN VIVO EXPERIMENTS GUIDELINES METHODS SUPPLEMENT

Study Design

- The groups being compared were control, cowpea mosaic virus (CPMV), cryoablation (Cryo), and cryoablation plus CPMV (Cryo + CPMV), as detailed in the Materials and Methods section of the manuscript.
- The experimental unit was individual mice.

Sample Size

- Control
  - Total N = 11: 8 for primary tumor size assessment (of these 8, 5 had appropriate contralateral tumor engraftment), 2 for flow cytometry, and 1 for histology.
- CPMV
  - Total N = 12: 8 for primary tumor size assessment (of these 8, 5 had appropriate contralateral tumor engraftment), 2 for flow cytometry, and 2 for histology.
- Cryo
  - Total N = 12: 8 for primary tumor size assessment (of these 8, 6 had appropriate contralateral tumor engraftment), 2 for flow cytometry, and 2 for histology.
- Cryo + CPMV
  - Total N = 14: 10 for primary tumor size assessment (of these 10, 8 had appropriate contralateral tumor engraftment), 2 for flow cytometry, and 2 for histology.
- The total number of animals included for analysis was 49.
  - A total of 60 animals received tumor injections; however, 11 were excluded per exclusion criteria described in the following section.
- The sample size was calculated using G*Power 3.1 (Heinrich Heine University, Düsseldorf, Germany), with an effect size of 0.80 estimated from pilot data, an error probability of 0.05, and a power of 0.85, yielding a calculated total sample

size of 8 per group plus 4 mice to account for engraftment failure and another 4 mice for histological/flow cytometric analysis for a sample size of 15 per group.

Inclusion and Exclusion Criteria

- A priori exclusion
  - No tumor or a tumor volume of <85 mm^3 on Day 0 of treatment (considered engraftment failure). Mice with a primary tumor that did meet the criteria but a secondary tumor that did not meet the criteria were still treated, but only the primary tumor was included for analysis in this case.
  - Mice whose deaths were related to intervention in the immediate periprocedural period (24 hours).
- Exclusion by experimental group
  - Control
    - Four were excluded for pretreatment primary tumor volumes of <85 mm^3.
  - CPMV
    - Two were excluded for pretreatment primary tumor volumes of <85 mm^3.
    - One was excluded for death immediately after treatment.
  - Cryo
    - Three were excluded for pretreatment primary tumor volumes of <85 mm^3.
  - Cryo + CPMV
    - One was excluded for pretreatment primary tumor volume of <85 mm^3.

Randomization

- Randomization to treatment groups was performed after tumor engraftment using a random number generator.
- There was no specific order of treatment during a treatment session or for tumor measurements.
- All animals from a single cage were usually, but not always, subject to intervention before moving onto the next cage.

Blinding

- The experimenter was blinded to group assignment when making tumor measurements.

- Blinding could not occur for treatment given technique used for immunostimulant administration and cryoablation.
- Blinding did not occur during data analysis.

Outcome Measures

- The outcome measures included tumor size, tumor immune cell infiltration by flow cytometry and immunohistochemistry, and serum cytokines/chemokines.
- Mice were sacrificed if the tumor volume measured >1 cm^3.
  - In addition, daily health checks were performed by the On Campus Veterinary Service. Mice were inspected for signs of decreased appetite, impaired ambulation, tachypnea, infection, lethargy, ruffled fur, hunched posture, bleeding, central nervous system disturbances, diarrhea or constipation, or muscle atrophy. Mice showing any of these signs were reported to the veterinarian, and their recommendations were followed, including sacrificing the animal if determined to be moribund. However, no mice in this experiment met any of these criteria.
- The primary outcomes measure was tumor growth.

Statistical Methods

- Statistical comparisons for tumor growth, flow cytometry, and histology were performed using 1-way analysis of variance.
- Statistical comparisons for enzyme-linked immunosorbent assay were performed using 2-way analysis of variance.
- GraphPad Prism 9 (San Diego, California) was used for all statistical calculations.

Experimental Animals

- All animals used were male unmodified C57BL/6J from The Jackson Laboratory (Bar Habor, Maine). They were started on a nonalcoholic steatohepatitis diet at 8–10 weeks of age and continued this for at least 4 weeks prior to tumor injections.

Experimental Procedures

- Further details are shown in the Materials and Methods section, “Ultrasound-Guided Percutaneous Cryoablation and Intratumoral CPMV Injection” subsection, of the manuscript.

RESULTS

Tables E2 and E3 (available online at www.jvir.org) present the additional descriptive statistics.

ABBREVIATIONS

CPMV	cowpea mosaic virus
HCC	hepatocellular carcinoma
IHC	immunohistochemistry
IL	interleukin
ISV	in situ vaccination
NK	natural killer
PBS	phosphate-buffered saline
TAA	tumor-associated antigen
TIL	tumor-infiltrating lymphocyte
TME	tumor microenvironment
US	ultrasound

REFERENCES

1. Bray F, Ferlay J, Soerjomataram I, Siegel RL, Torre LA, Jemal A. Global cancer statistics 2018: GLOBOCAN estimates of incidence and mortality worldwide for 36 cancers in 185 countries. CA Cancer J Clin 2018; 68: 394–424. [PubMed: 30207593]
2. Pang YL, Zhang HG, Peng JR, et al. The immunosuppressive tumor microenvironment in hepatocellular carcinoma. Cancer Immunol Immunother 2009; 58:877–886. [PubMed: 18941744]
3. Jansen MC, van Hillegersberg R, Schoots IG, et al. Cryoablation induces greater inflammatory and coagulative responses than radiofrequency ablation or laser induced thermotherapy in a rat liver model. Surgery 2010; 147:686–695. [PubMed: 20042207]
4. den Brok MH, Sutmuller RP, Nierkens S, et al. Efficient loading of dendritic cells following cryo and radiofrequency ablation in combination with immune modulation induces anti-tumour immunity. Br J Cancer 2006; 95: 896–905. [PubMed: 16953240]
5. Kumar AV, Patterson SG, Plaza MJ. Abscopal effect following cryoablation of breast cancer. J Vasc Interv Radiol 2019; 30:466–469. [PubMed: 30819495]
6. Uhlschmid G, Kolb E, Largiadèr F. Cryosurgery of pulmonary metastases. Cryobiology 1979; 16:171–178. [PubMed: 477364]
7. Joosten JJ, Muijen GN, Wobbes T, Ruers TJ. In vivo destruction of tumor tissue by cryoablation can induce inhibition of secondary tumor growth: an experimental study. Cryobiology 2001; 42:49–58. [PubMed: 11336489]
8. Banstola A, Jeong JH, Yook S. Immunoadjuvants for cancer immunotherapy: a review of recent developments. Acta Biomater 2020; 114: 16–30. [PubMed: 32777293]
9. Murray AA, Wang C, Fiering S, Steinmetz NF. In situ vaccination with cowpea vs tobacco mosaic virus against melanoma. Mol Pharm 2018; 15:3700–3716. [PubMed: 29798673]
10. Kerstetter-Fogle A, Shukla S, Wang C, et al. Plant virus-like particle in situ vaccine for intracranial glioma immunotherapy. Cancers (Basel) 2019; 11: 515. [PubMed: 30974896]
11. Wang C, Steinmetz NF. CD47 blockade and cowpea mosaic virus nanoparticle in situ vaccination triggers phagocytosis and tumor killing. Adv Healthc Mater 2019; 8:e1801288. [PubMed: 30838815]

12. Wang C, Fiering SN, Steinmetz NF. Cowpea mosaic virus promotes antitumor activity and immune memory in a mouse ovarian tumor model. Adv Ther (Weinh) 2019; 2:1900003. [PubMed: 33969181]
13. Shukla S, Jandzinski M, Wang C, et al. A viral nanoparticle cancer vaccine delays tumor progression and prolongs survival in a HER2+ tumor mouse model. Adv Ther (Weinh) 2019; 2:1800139. [PubMed: 33855164]
14. Patel R, Czapar AE, Fiering S, Oleinick NL, Steinmetz NF. Radiation therapy combined with cowpea mosaic virus nanoparticle in situ vaccination initiates immune-mediated tumor regression. ACS Omega 2018; 3:3702–3707. [PubMed: 29732445]
15. Alonso-Miguel D, Valdivia G, Guerrera D, et al. Neoadjuvant in situ vaccination with cowpea mosaic virus as a novel therapy against canine inflammatory mammary cancer. J Immunother Cancer 2022; 10:e004044. [PubMed: 35277459]
16. Hoopes PJ, Wagner RJ, Duval K, et al. Treatment of canine oral melanoma with nanotechnology-based immunotherapy and radiation. Mol Pharm 2018; 15:3717–3722. [PubMed: 29613803]
17. Koellhoffer EC, Steinmetz NF. Cowpea mosaic virus and natural killer cell agonism for in situ cancer vaccination. Nano Lett 2022; 22:5348–5356. [PubMed: 35713326]
18. Leong HS, Steinmetz NF, Ablack A, et al. Intravital imaging of embryonic and tumor neovasculature using viral nanoparticles. Nat Protoc 2010; 5: 1406–1417. [PubMed: 20671724]
19. Brown ZJ, Heinrich B, Greten TF. Establishment of orthotopic liver tumors by surgical intrahepatic tumor injection in mice with underlying non-alcoholic fatty liver disease. Methods Protoc 2018; 1:21. [PubMed: 31164564]
20. Zabransky DJ, Danilova L, Leatherman JM, et al. Profiling of syngeneic mouse HCC tumor models as a framework to understand anti-PD-1 sensitive tumor microenvironments. Hepatology 2023; 77: 1566–1579. [PubMed: 35941803]
21. Schindelin J, Arganda-Carreras I, Frise E, et al. Fiji: an open-source platform for biological-image analysis. Nat Methods 2012; 9:676–682. [PubMed: 22743772]
22. Huo Y, Chen WS, Lee J, Feng GS, Newton IG. Stress conditions induced by locoregional therapies stimulate enrichment and proliferation of liver cancer stem cells. J Vasc Interv Radiol 2019; 30:2016–2025.e5. [PubMed: 31208945]
23. Sabel MS. Cryo-immunology: a review of the literature and proposed mechanisms for stimulatory versus suppressive immune responses. Cryobiology 2009; 58:1–11. [PubMed: 19007768]
24. Shigeta K, Datta M, Hato T, et al. Dual programmed death receptor-1 and vascular endothelial growth factor receptor-2 blockade promotes vascular normalization and enhances antitumor immune responses in hepatocellular carcinoma. Hepatology 2020; 71:1247–1261. [PubMed: 31378984]
25. Wang C, Steinmetz NF. A combination of cowpea mosaic virus and immune checkpoint therapy synergistically improves therapeutic efficacy in three tumor models. Adv Funct Mater 2020; 30:2002299. [PubMed: 34366758]
26. Hiraoka N Tumor-infiltrating lymphocytes and hepatocellular carcinoma: molecular biology. Int J Clin Oncol 2010; 15:544–551. [PubMed: 20924634]
27. Khan SY, Melkus MW, Rasha F, et al. Tumor-infiltrating lymphocytes (TILs) as a biomarker of abscopal effect of cryoablation in breast cancer: a pilot study. Ann Surg Oncol 2022; 29:2914–2925. [PubMed: 35094188]
28. Ding W, Xu X, Qian Y, et al. Prognostic value of tumor-infiltrating lymphocytes in hepatocellular carcinoma: a meta-analysis. Medicine (Baltimore) 2018; 97:e13301. [PubMed: 30557978]
29. Cao Z, Fu B, Deng B, Zeng Y, Wan X, Qu L. Overexpression of chemokine (C-X-C) ligand 1 (CXCL1) associated with tumor progression and poor prognosis in hepatocellular carcinoma. Cancer Cell Int 2014; 14:86. [PubMed: 25298747]
30. Susek KH, Karvouni M, Alici E, Lundqvist A. The role of CXC chemokine receptors 1–4 on immune cells in the tumor microenvironment. Front Immunol 2018; 9:2159. [PubMed: 30319622]

RESEARCH HIGHLIGHTS

- Combined treatment of cryoablation with cowpea mosaic virus–derived nanoparticles inhibited tumor growth in a subcutaneous mouse model of liver cancer compared with control tumors (change in volume, 1.6-fold ± 0.9 vs 6.3-fold ± 0.5; $P < .0001$).
- Combined treatment caused a modest abscopal effect, with delayed growth of a contralateral untreated tumor (9.2-fold ± 0.9 vs 17.8-fold ± 2.1; $P = .01$).
- These effects were associated with enrichment of native and adaptive immune cells, especially in the center of treated tumors, and with reduced expression of CXCL1, suggesting a shift from an immunologically cold to hot tumor milieu.

STUDY DETAILS

Study type:

Animal study

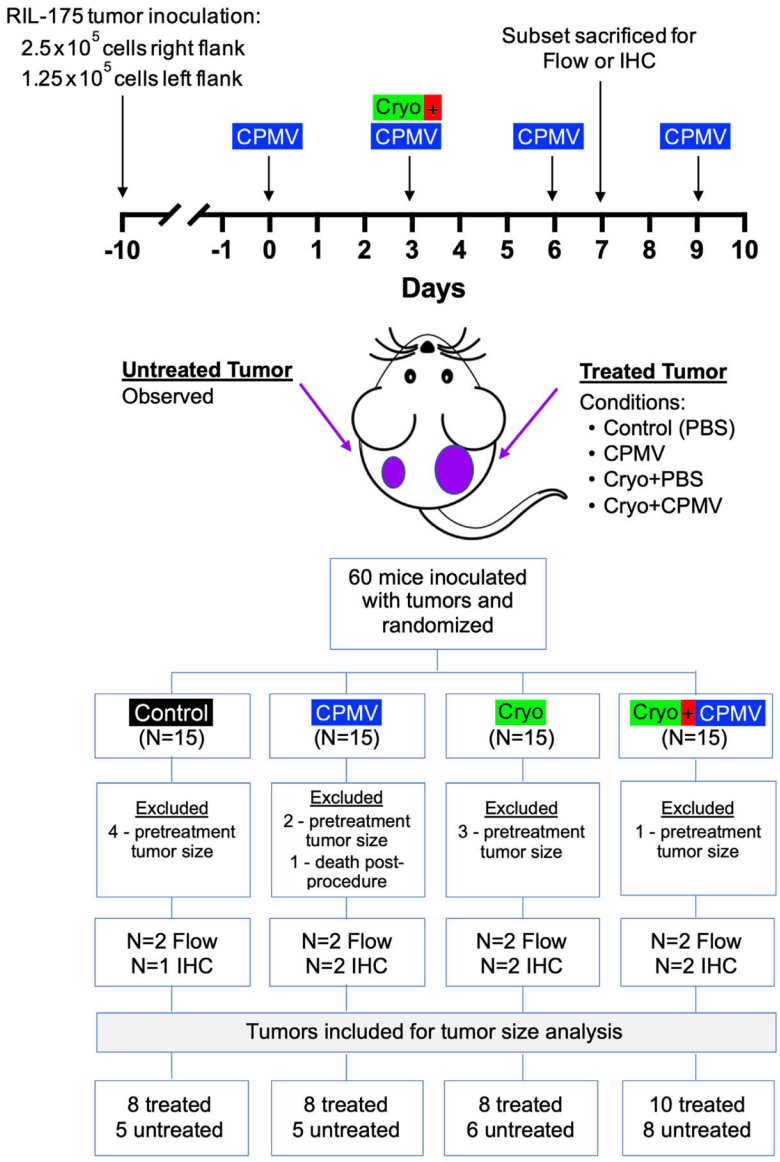

Figure 1.

Study design and treatment schedule. The treated tumor was subjected to 1 of the following 4 conditions: (*a*) phosphate-buffered saline (PBS) (Control), (*b*) cowpea mosaic virus–treated only (CPMV), (*c*) cryoablation only (Cryo), and (*d*) cryoablation plus CPMV–treated (Cryo + CPMV). The untreated tumor was observed. Mice were excluded if the primary tumor volume measured <85 mm^3 at the time of treatment. Tissues were analyzed by flow cytometry (Flow) or immunohistochemistry (IHC).

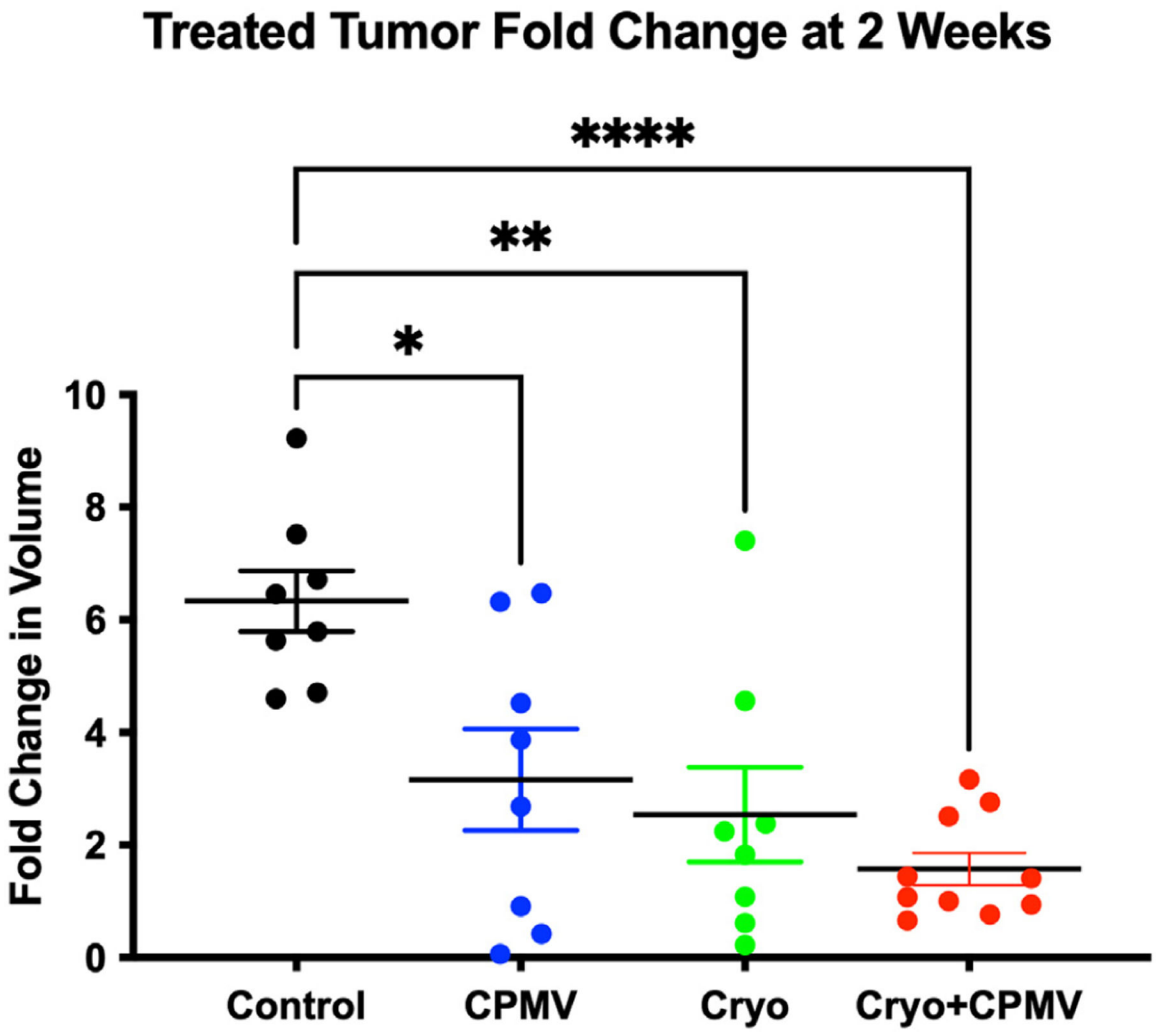

Figure 2.

Cryoablation only (Cryo) and cowpea mosaic virus–treated only (CPMV), alone or in combination, significantly retarded treated tumor growth. Fold change in tumor size at 2 weeks after treatment initiation: the CPMV, Cryo, and cryoablation plus CPMV–treated (Cryo + CPMV) groups demonstrated significantly slower growth compared with that in the control group (black). Cryo + CPMV resulted in marked reduction of tumor growth compared with that in the control group (1.6 ± 0.9 vs 6.3 ± 0.5, $P < .0001$). This change did not reach significance compared with CPMV or Cryo alone. The fold change growth of CPMV was 3.2 ± 2.6 ($P = .01$), and that of Cryo was 2.5 ± 2.4 ($P = .002$). The asterisks indicate statistical significance: *$P < .05$, **$P < .01$, and ****$P < .0001$.

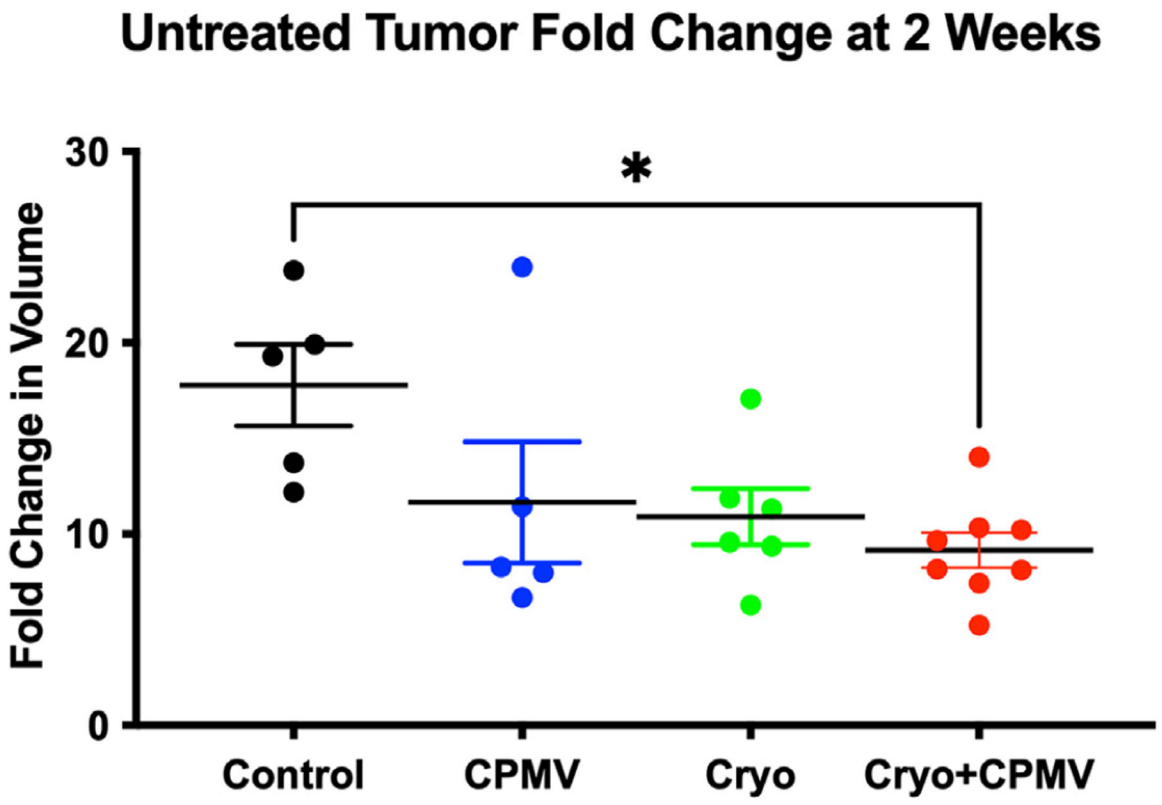

Figure 3.

The cryoablation plus cowpea mosaic virus–treated (Cryo + CPMV) group significantly retarded untreated tumor growth. The fold change in untreated tumor volumes at 2 weeks compared with the baseline demonstrated growth suppression of the untreated tumor in the Cryo + CPMV group (red) compared with that in the control group (black) (9.2 ± 0.9 vs 17.8 ± 2.1, $P = .01$); the single-arm groups trended toward growth retardation without meeting statistical significance. Time course data were analyzed using repeated-measures 2-way analysis of variance, and tumor size at 2 weeks was analyzed using 1-way analysis of variance with the Tukey post hoc test. The asterisk indicates statistical significance: $*P < .05$. CPMV = cowpea mosaic virus–treated only; Cryo = cryoablation only.

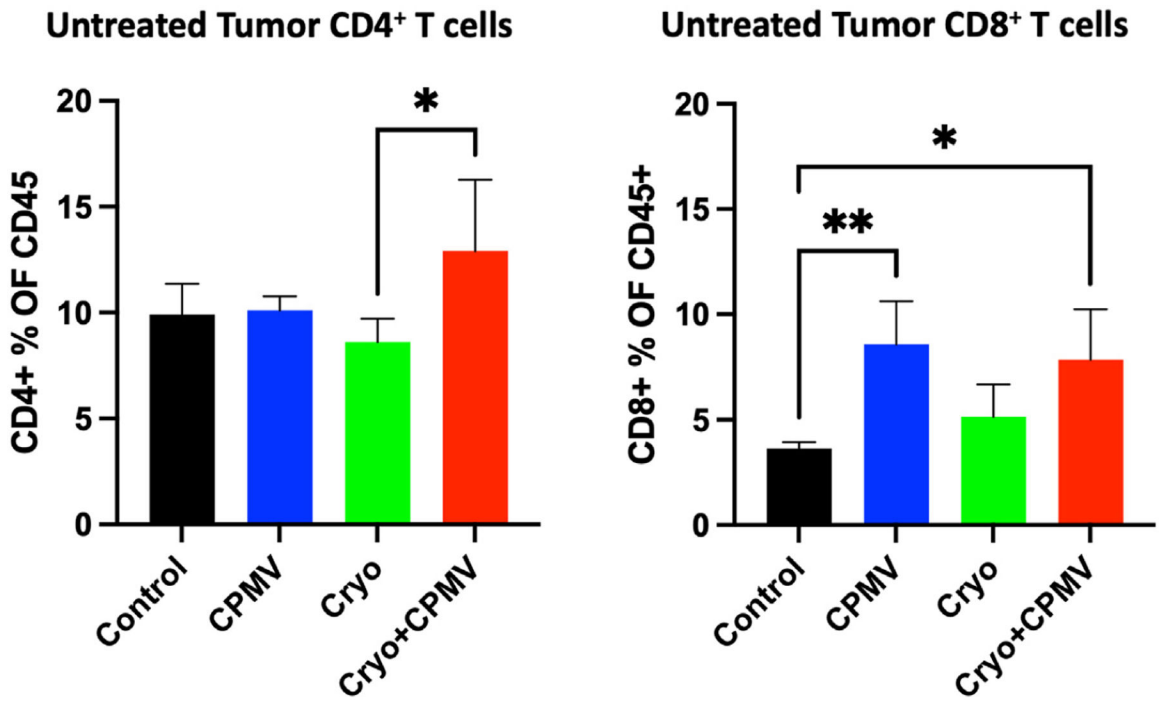

Figure 4.

Flow cytometry revealed enrichment of $CD4^+$ and $CD8^+$ T cells in the untreated tumors with cryoablation plus cowpea mosaic virus (Cryo + CPMV). The $CD4^+$ cell levels increased in the Cryo + CPMV group compared with those in the cryoablation only (Cryo) group in the untreated tumor (12.9% vs 8.6%, $P = .03$). The $CD8^+$ cell levels increased in both the cowpea mosaic virus–treated only (CPMV) (8.6%, $P = .005$) and Cryo + CPMV (7.8%, $P = .03$) groups compared with those in the control group (3.6%). Immune cell enrichment was analyzed using 1-way analysis of variance with Tukey post hoc tests. The asterisks indicate statistical significance: $*P < .05$, and $**P < .01$.

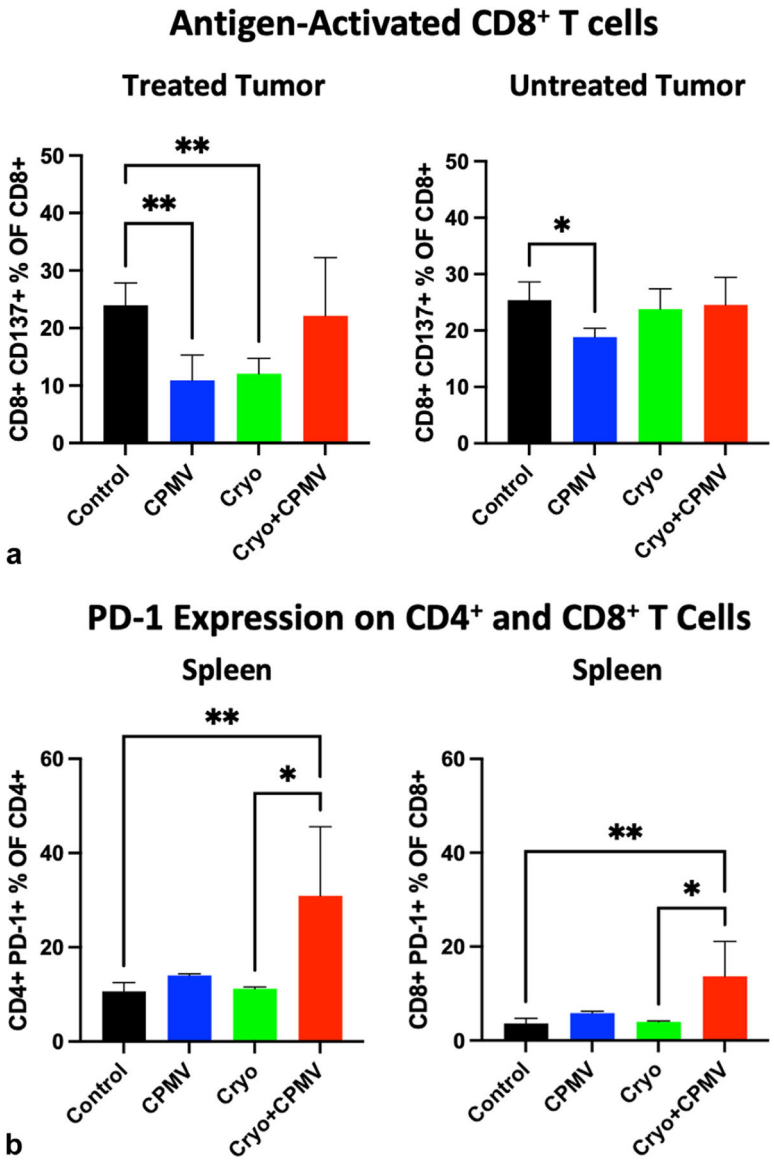

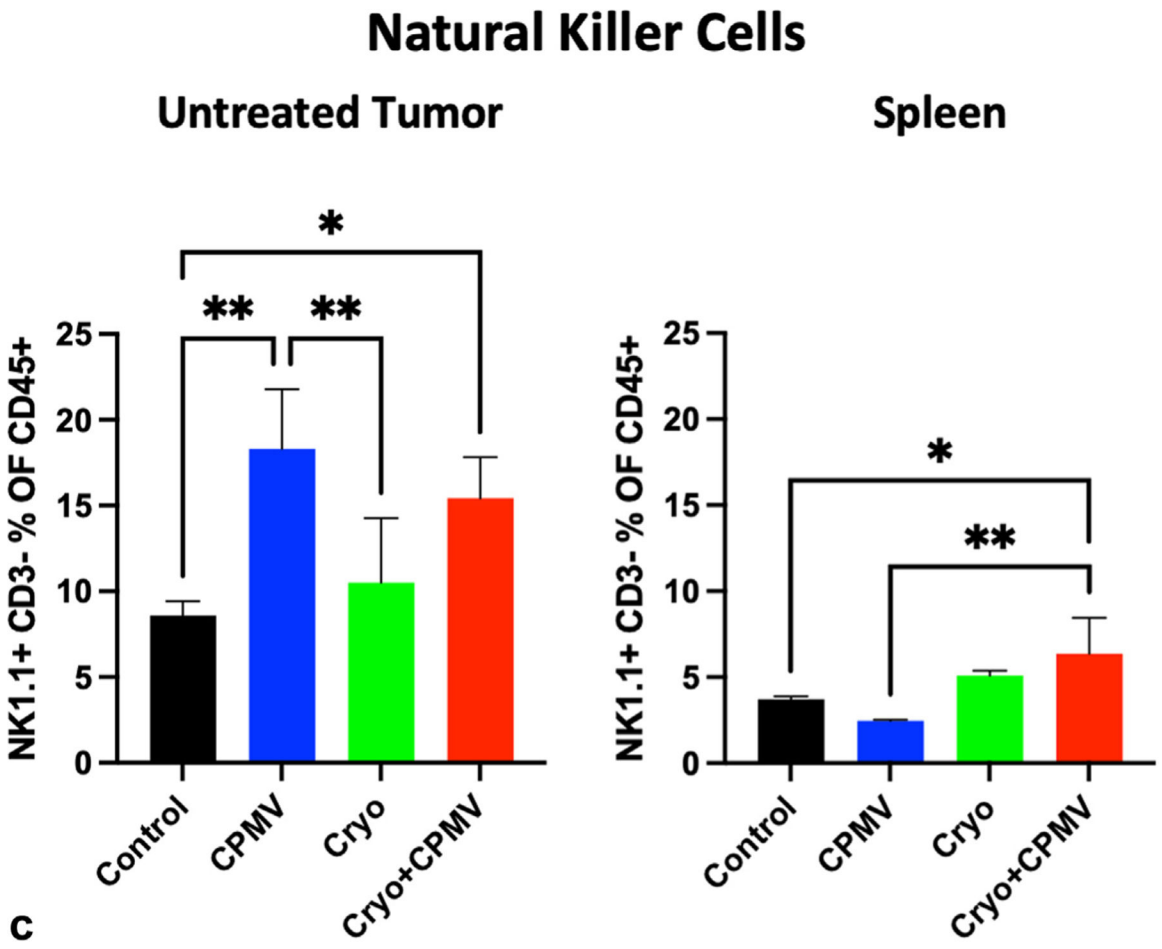

Figure 5.

Flow cytometry revealed that cowpea mosaic virus–treated only (CPMV) or cryoablation only (Cryo) could suppress antigen-activated $CD8^+$ T cells and cryoablation plus cowpea mosaic virus (Cryo + CPMV) increased the natural killer cell levels in the untreated tumors and spleens but with upregulation of PD-1. **(a)** The levels of antigen-activated CD8+ T cells decreased in the treated tumors of the CPMV (10.9% vs 24.0%, $P = .01$) and Cryo (12.0% vs 24%, $P = .01$) groups and the untreated tumors in the CPMV group (18.8% vs 25.4%, $P = .04$) compared with those of in the control group. Cryo + CPMV did not demonstrate such inhibition. **(b)** Combined treatment demonstrated that immune exhaustion with PD-1 expression on both $CD4^+$ cells and $CD8^+$ cells in the spleen increased with Cryo + CPMV compared with either control ($CD4^+$, 30.9% vs 10.6%; $P = .007$, and $CD8^+$, 13.7% vs 3.6%; $P = .008$) or Cryo ($CD4^+$, 30.9% vs 11.2%; $P = .03$, and $CD8^+$, 13.7% vs 4.0%; $P = .04$). **(c)** Natural killer (NK) cells were enriched in both the untreated tumors (15.4% vs 8.6%, $P = .04$) and spleens (6.3% vs 3.7%, $P = .01$) of the Cryo + CPMV group compared with control group. Untreated tumors also had enriched NK cells in the CPMV group compared to control group (18.3% vs 8.6%, $P = .002$). Full flow cytometry data are shown in Figure E4 (available online at www.jvir.org). Immune cell enrichment was analyzed using 1-way analysis of variance with Tukey post hoc tests. The asterisks indicate statistical significance: $*P < .05$, and $**P < .01$.

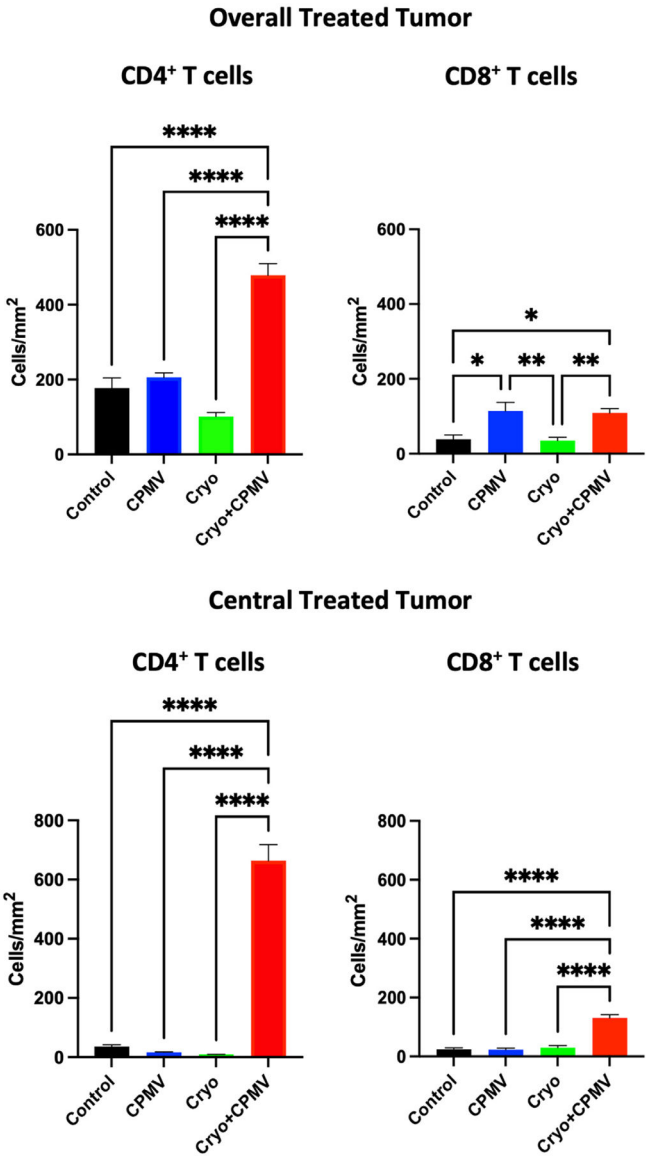

Figure 6.

The treated tumors of cryoablation plus cowpea mosaic virus–treated (Cryo + CPMV) mice demonstrated increased overall and tumor-infiltrating $CD4^+$ and $CD8^+$ cytotoxic T cell levels. The levels of tumor-infiltrating $CD4^+$ and cytotoxic $CD8^+$ in treated tumors were categorized on immunohistochemistry by overall and central distributions. Cells were counted from 5–10 low-power fields from 3 sections from each mouse. Immune cell levels were analyzed using 1-way analysis of variance with Tukey post hoc tests. The asterisks indicate statistical significance: $*P < .05$, $**P < .01$, and $****P < .0001$. CPMV = cowpea mosaic virus–treated only; Cryo = cryoablation only.

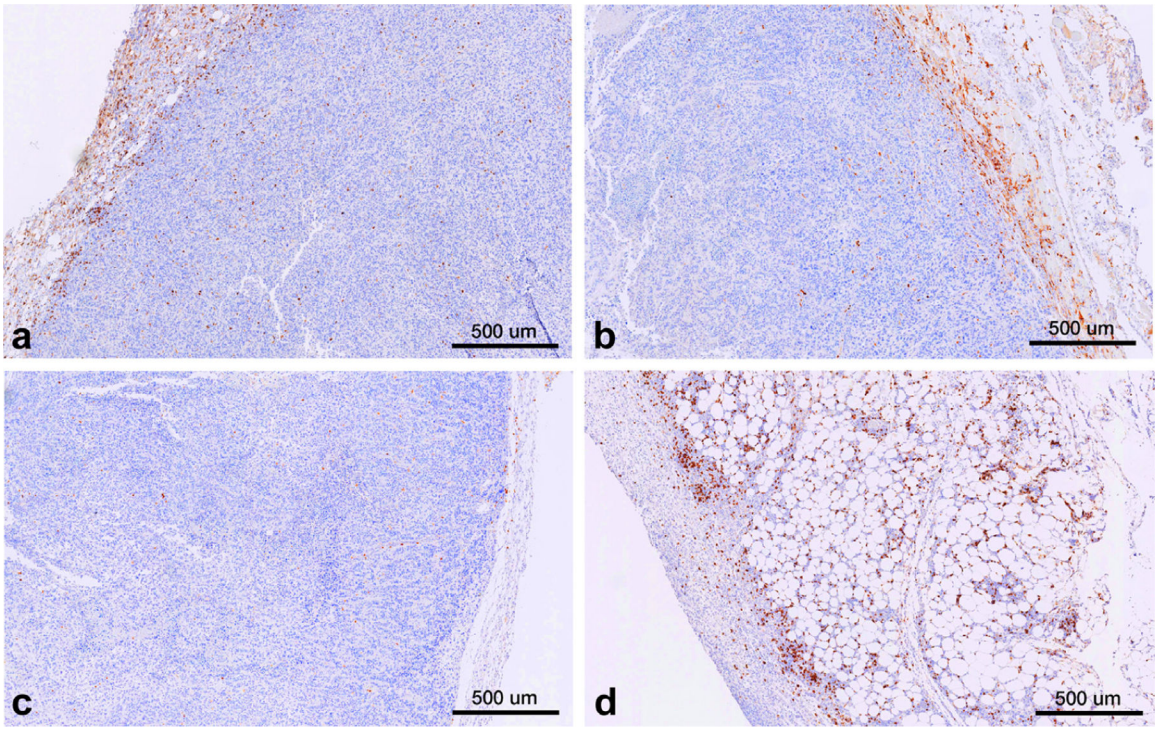

Figure 7.

Compared with those of **(a–c)** other groups, tumors treated with **(d)** cryoablation plus cowpea mosaic virus (Cryo + CPMV) demonstrated greater infiltration of helper T cells (CD4+) and fat necrosis. Representative immunohistochemistry images of treated tumors at 5× magnification demonstrating $CD4^+$ staining of treated tumors of the following groups: (*a*) Control, (*b*) cowpea mosaic virus–treated only (CPMV), (*c*) cryoablation only (Cryo), and (*d*) Cryo + CPMV. Control and CPMV tumors demonstrated $CD4^+$ lymphocyte accumulation at the periphery of the tumors (brown stain) while there was a paucity of CD4+ cells in Cryo tumors. Cryo + CPMV tumors demonstrated increased levels of $CD4^+$ lymphocytes throughout the tumor, with diffuse fat content (clear ovoid spaces).